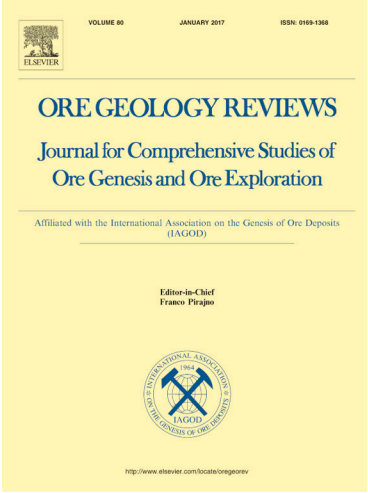

Crustal architecture studies in the Iranian Cadomian arc: Insights into source, timing and metallogeny

Yusef Vesali, Fatemeh Sepidbar, Richard M. Palin, Massimo Chiaradia

PII: S0169-1368(21)00306-1
DOI: https://doi.org/10.1016/j.oregeorev.2021.104280
Reference: OREGEO 104280

To appear in: *Ore Geology Reviews*

Received Date: 10 November 2020
Revised Date: 26 April 2021
Accepted Date: 3 June 2021

Please cite this article as: Y. Vesali, F. Sepidbar, R.M. Palin, M. Chiaradia, Crustal architecture studies in the Iranian Cadomian arc: Insights into source, timing and metallogeny, *Ore Geology Reviews* (2021), doi: https://doi.org/10.1016/j.oregeorev.2021.104280

Crustal architecture studies in the Iranian Cadomian arc: Insights into source, timing and metallogeny

Yusef Vesali[a], Fatemeh Sepidbar*[b], Richard M. Palin[c], Massimo Chiaradia[d]

[a]Department of Geology, Faculty of Science, University of Tehran, Tehran, 14155-64155, Iran

[b]School of Earth Sciences, Damghan University, Damghan 36716-41167, Iran

[c]Department of Earth Sciences, University of Oxford, Oxford, UK

[d]Department of Mineralogy, Section of Earth and Environmental Sciences, University of Geneva, Geneva, Switzerland

Abstract

The Jalal Abad magmatic rocks, situated at the southern edge of the Saghand-Bafgh-Zarand district, include a thick pile of Cadomian extrusive and pyroclastic units intruded by younger granitoid stocks. New zircon U–Pb ages show eruptions at ~552 Ma, followed by emplacement of granodiorite at ~537 Ma. The Jalal Abad magmatic rocks have typical high-K and shoshonitic signatures, and are characterized by enrichment in large-ion lithophile elements (LILEs) and depletion in high-field-strength elements (HFSE). Zircon εHf(t) from the Jalal Abad magmatic rocks ranges from +3.9 to −3.9 for volcanic rocks and −1.2 to +8.1 for granodiorite. Zircon $\delta^{18}O$ values for the Jalal Abad are variable from +5.1 to +8.8‰, progressively higher than those of mantle-derived melts. The whole-rock εNd(t) values range between −7.7 to −7.4 for granodiorite, −4.6 to −3 for volcanic rocks and −6.2 to −8.2 for ignimbrites/tuff. The whole-rock Nd and zircon Hf crustal model ages (T_{DM}^{C}) for the Jalal Abad magmatic rocks range between 0.8 and 2.3 Ga. All of the Jalal Abad magmatic rocks have quite similar trace element patterns, and slightly different whole-rock Nd and zircon Hf isotopic composition, indicating the involvement of the thick continental crust during the formation of these rocks. Modeling of zircon Hf–O data, bulk-rock trace elements, and Sr–Nd isotopes suggest the magmas were generated by interaction of mantle–derived melts with thick continental crust through assimilation/fractional crystallization (AFC) processes. However, crustal architecture studies in the Iranian Cadomian arcs show that AFC processes were more

important during the Mesoarchean–Early Neoproterozoic (3000–1000 Ma), whereas juvenile magmas became increasingly important to the Cadomian (600–500 Ma) magmatism. Early Cambrian intrusive magmas seemingly intruded sedimentary sequences in the study region and provided magmatic constituents and a heat source for hydrothermal processes and mineralization.

Keywords: Zircon U–Pb dating, Cadomian magmatism, AFC processes, Iran.

Introduction

Magmatic rocks associated with the Cadomian orogeny are thought to have formed at the northern border of Gondwana along an active continental margin at c. 750−540 Ma (e.g. Linnemann et al., 2008 and references therein) and were later affected by Early Paleozoic rifting at ca. 530–485 Ma (e.g. Sánchez-García et al., 2008; Nance et al., 2010 and references therein) associated with opening of the Rheic Ocean. Geochemical data suggest that these Cadomian plutons formed due to subduction of the Proto-Tethys Ocean underneath the northern margin of Gondwana during the Late Neoproterozoic. They are often thought to be fragments rifted away from the Arabian–Nubian Shield (ANS), which is dominated by Neoproterozoic continental crust formed between 900 and 580 Ma through the accretion of intra-oceanic arcs.

Iran was located on the northeastern margin of Gondwana during the Neoproterozoic and Early Cambrian (Hassanzadeh et al., 2008; Balaghi Einalou et al., 2014). The widespread uniformity of Ediacaran strata that cover the central basement of Iran suggests that it was once part of an undivided Paleozoic ANS platform belonging to Gondwana (e.g., Stöcklin, 1968, 1974). There was relatively simultaneous emplacement of crystalline Cadomian magmatic rocks with various sizes distributed in the Golpayegan (western Cadomian exposure), Khoy-Salmas, Zanjan-Takab (northwestern Cadomian exposure), Torud, Taknar (north-eastern Cadomian exposures) and Saghand-Bafgh-Zarand (central-southeast Cadomian exposures) regions of Iran (Moghadam et al., 2017c) at this time (Fig. 1).

The central-southeast Cadomian magmatic rocks of Iran are mostly composed of orthogneiss, amphibolite, granite and metagranite, with sparse mafic rocks (e.g. Hassanzadeh et al., 2008; Moghadam et al., 2015a). In particular, zircon U–Pb ages from these lithologies have revealed a distinct magmatic peak during the Late Neoproterozoic–Early Cambrian, from 610 Ma to 520

Ma (e.g. Ramezani and Tucker, 2003; Hassanzadeh et al., 2008; Moghadam et al., 2015a; Rossetti et al., 2015; Badr et al., 2017).

Iron oxide deposits are commonly linked to volcanic and sub-volcanic rocks in volcanic–plutonic belts, with many Proterozoic to Cenozoic occurrences known worldwide. Well-documented examples include magnetite deposits (e.g., El Romeral; Bookstrom, 1977), magnetite–apatite (Kiruna-type) deposits (e.g., El Laco; Nyström and Henríquez, 1994), and magnetite deposits with economic Cu and Au mineralization (the IOCG *sensu stricto* deposits, described by Chen et al., 2010a,b for Marcona-Mina Justa, in the Chilean iron belt). Such deposits are genetically associated with intermediate calc-alkaline magmas in a volcanic-plutonic continental arc setting. The source of these deposits has been the issue of much research, with both magmatic models that confirm immiscible iron oxide-rich melts (e.g., Nyström and Henríquez, 1994;) and hydrothermal models (e.g. Ménard, 1995; Sillitoe, 2003) being proposed, although their origin remains contentious.

The Saghand-Bafgh-Zarand district is, a world-class iron oxide province located in the central Cadomian magmatic belt, and is a well-known iron-apatite province containing iron oxide ± Cu ± Au ± Bi ± Co and Kiruna deposits related to Cadomian magmatic systems (Ramezani and Tucker, 2003). This district consists of massive magnetite and magnetite-apatite ores hosted in Early Cambrian sequences of sedimentary and volcanic rocks (lavas, pyroclastic and epiclastic rocks).

The Jalal Abad magmatic complex and associated iron oxide mineralization is located in the southern part of the Saghand-Bafgh-Zarand district. It is of particular interest in terms of its large size and high grade, as well as its characteristic ore and mineral associations (i.e. ± Cu ± Au ± Bi ± Co within magnetite). Iron mineralization at Jalal Abad is likely of magmatic origin with subordinate hydrothermal overprinting (Mehrabi et al., 2019). Previous studies of Jalal Abad have focused on its isotope characteristics, microthermometry and the chemistry of fluid inclusions in the deposit (Mehrabi et al., 2019). However, the nature and tectonic affinity of the volcanic host rock is still controversial and competing models for its genesis include a rift-related origin (Samani, 1988, 1998; Daliran, 1990, 1999, 2002; Förster and Jafarzadeh, 1994) and a subduction-related origin (Ramezani and Tucker (2003). Furthermore, some earlier studies (e.g. Vesali et al., 2020; Vesali et al., 2018) addressed the genesis of Paleozoic alkaline intrusive rocks of Jalal Abad iron deposits and focused mainly on the age of magma emplacement in the Paleozoic extension zone, whereas basic descriptions of the geology and

mineralogy of the Cadomian volcanic rocks and associated deposits are rare, as well as the ages of formation and tectonic setting being uncertain.

To improve tectonic models for the evolution of the Central Iranian Terrane, new constraints on the geological processes, ages and the original positions and geotectonic settings of Cadomian volcanic rocks are needed. In this paper, the geology, paragenetic sequence, mineralization styles, and mineral chemistry of the Jalal Abad deposit are described in detail. New whole-rock geochemical and Nd–Sr isotopic analyses, U–Pb zircon ages and zircon Hf–O isotopic compositions are represented for the Jalal Abad volcanic rocks of central Iran, which is a typical example of Cadomian magmatic exposures in the Saghand-Bafgh-Zarand district. These data are then combined to provide preliminary constraints on the genesis of the Jalal Abad deposit.

2. Regional geology and field observations

The Saghand-Bafgh-Zarand district is located within the Kashmar-Kerman Tectonic zone (KKTZ), which is situated between the Yazd block to the west and the Tabas block to the east. The regional geological and tectonic setting of the KKTZ has been described extensively (e.g., Charvet et al., 2011; Gao et al., 2009) and its structural architecture is regarded to have developed due to subduction of the Proto-Tethys Ocean. The zircon Hf and whole-rock Nd isotopic compositions of KKTZ magmatic rocks suggest that they formed during mixing between juvenile melts derived from mantle and old continental crust or/partial melting of older continental crust (Abbo et al., 2015; Moghadam et al., 2015; Moghadam et al., 2017a).

The KKTZ contains variably deformed and fault-bound Neoproterozoic supracrustal rocks of the Boneh-Shurow and Task complexes and Early Cambrian volcano-sedimentary unit. During subduction of the Proto-Tethys Ocean, Early Cambrian arc magmatism produced many volcanic and intrusive complexes in the KKTZ (e.g., Ramezani and Tucker, 2003), including the Rizu-Desu Formations, which are composed predominantly of greywackes and a volcano-sedimentary unit of siltstones, tuffaceous sandstones, thick iron-rich layers, tuffites, intermediate to felsic volcanic rocks, tuffaceous limestones and conglomerates (Horton et al., 2008; Ramezani and Tucker, 2003). The Rizu-Dezu Formations are widespread throughout the KKTZ, ranging in age from Middle Neoproterozoic (760 ± 120 Ma), Late Neoproterozoic (595 Ma) (Huckriede and others, 1962) to Early Cambrian (528 Ma) (Horton et al., 2008; Ramezani and Tucker, 2003). It is the main host to various styles of mineralization in the KKTZ, including iron oxide-Cu-Au ± Bi-Co mineralization (Mehrabi, et al., 2019).

Several iron deposits (e.g., Chador Malu, Se-Chahun, Esfordi, Choghart, and Jalal Abad) have been explored in the past decade during geological surveys through the KKTZ. These iron deposits collectively form a 200-km-long and 10–20-km-wide iron belt, termed the Saghand-Bafgh-Zarand district (Fig. 1). Most iron deposits are hosted by rocks of the Rizu-Desu Formation. The iron mineralization is characterized by high-grade magnetite ores that are accompanied by wide alteration zones of sodic-calcic and potassic alteration, and sericitization and silicification metasomatism.

Jalal Abad magmatic rocks from the southeast Saghand-Bafgh-Zarand district in Iran occupy an exposed area of ~50 km^2 (Fig. 2). The oldest units in the Jalal Abad complex are Ediacaran sandstones and shales of the Morad series (Fig. 2), based on radiometric dating, stratigraphic position and different Ediacaran and Cambrian fossils (Horton et al., 2008; Ramezani and Tucker, 2003). Cadomian clastic rocks of the Morad series are overlain with Cadomian clastic rocks of the Rizu Formation (Fig. 2). A U–Pb zircon age of 537.5 ±1.6 Ma for dacites and rhyolites from the Zarand, north of Jalal Abad, indicates an Early Cambrian age of formation (Sepidbar et al., 2020).

The Rizu Formation is the main host rock of the Jalal Abad deposit (Vahdati, 1995) and is subdivided into two main units. The lower units mainly consist of a basal grey, green to pink greywacke sandstone member, which has a limited surfce exposure in the western sector of the mining area and is known as the “floor sandstone” (Gotlov and Esev, 1976). This unit is conformably overlain by a thick sequence of volcano-sedimentary rocks including siltstone, tuff sandstone, thick magnetite layers, tuffites, intermediate to acid volcanic rocks, tuffaceous limestone and conglomerate. The main distinctive feature of this unit is a sharp facies change from detrital to marine deposit, indicative of a change of depositional environment (Gotlov and Esev, 1976). This volcano-sedimentary unit covers a considerable area in the eastern and southern part of mineralized zone, where it reaches a thickness of more than 1100 m (Fig. 2a). The volcanic rocks of this unit include rhyolite, rhyodacite, dacite, ignimbrite and pyroclastic rocks (Gotlov and Esev, 1976). Rhyolite occurs as isolated dome-like outcrops in the eastern and southern mineralized zones, and are probably equivalents to silicic volcanic units of the Kahar and Qara–Dash Formations in N–NW Iran (Moghadam et al., 2017c). Rhyolitic to rhyodacitic tuffs and dolomite occur intercalated between rhyolitic (flow) layers (Fig. 3a and b). Several ignimbrite sheets also occur in the vicinity of the rhyolites, and commonly have gradational contacts with rhyolites and rhyodacites. The ignimbrite shows a variety of coloration from gray, grayish green to pink and are characterized by several lenticular and

flattened fiammes ranging in diameter from 2 to 6 cm (Fig. 3c). Fiamme usually indicate a single compactional flattening event; however, in some welded tuffs, the fiamme are stretched and show a lineation parallel to the flow foliation, which indicates secondary displacement of the tuff during welding (rheomorphism) (Cas and Wright, 1987). Dusty quartz and feldspar infills in the matrix, pumice cavities and reticulated veinlets probably formed during percolation of fluids through ignimbrites during their devitrification.

The tuff and ignimbrite change laterally to tuffite and sandy tuffs, which are distal expressions of this volcanism, and show that units in this stage of the Cadomian arc formed near to sea level. Evidence of both subaerial and submarine extrusion exists in the form of fluvially reworked crystal tuff and lapillistone with inverse grading as well as hyaloclastite, respectively.

The thick sequences (~350–400 m) of Lower Cambrian dolomitized limestone overlie the older Rizu-series , and form a part of the Desu series, which is stratigraphically equivalent to the Early Cambrian Soltanieh dolomite formation in the Alborz-Azerbaijan region (Mehrabi et al., 2014). Small intrusive bodies of granodiorite, gabbro, diorite and diabasic dykes were emplaced into the volcano-sedimentary unit and Early Cambrian dolomites and produced a narrow contact metamorphic aureole. Granodiorites occur as small stocks in the southwest of the Jalal Abad domain and crosscut rocks of both the Ediacaran Morad series and Early Cambrian sedimentary rocks of the Rizu Formation (Fig. 3e). The small and irregular (~200 × 300 m) coarse-grained mafic to intermediate rocks are widespread in the southern and southeastern parts of the mineralized area, and intrude across Early Cambrian sedimentary rocks of the Rizu Formation. The NW-SE-trending mafic dykes and sills are some of the main magmatic rocks in the mineralized area and cut all lithological units. The dykes are mostly confined to tectonized zones and widely vary in thickness, but most are up to 1 km long and 2–25 m wide (Gotlov and Esev, 1976).

3. Jalal Abad mine geology

The Jalal Abad ore body is lens-shaped and trends NW-SE across an area of open folding. Based on its magnetic anomaly, the ore body is approximately 2500 m long. In the Jalal-Abad, iron oxide-Cu-Au ± Bi-Co mineralization is identified mainly from borehole samples. The cross section of the deposit (Fig. 2b) is based on exploratory drill cores that demonstrate iron mineralization down to 486 m below the surface with variable oxidation state depending on topographic location and fault displacements. The surface outcrop of iron ore is limited to the northwestern part of the body. The ore-bearing horizon is 250–180 m thick and consists of

chloritized siltstone, sandy siltstone, rhyodacitic tuff and dolomite (Fig. 3f) with iron oxide and sulfide mineralization. Siltstone, sandstone, conglomerate, rhyodacitic ignimbrite, rhyodacitic tuff, dolomite, breccia and alluvium occur above the ore body. There is no iron oxide mineralization in this upper zone (Fig. 2b).

Most of the iron oxide ore bodies, particularly the large ones, are hosted by Early Cambrian volcano-sedimentary units of sandy siltstone, dolomite and felsic volcanic rocks (Fig. 2), which are intruded by younger diorite and gabbro sills or dykes (Fig. 2). Rhyodacitic tuff and ignimbrite and rhyodacite lavas are widespread in the central and southeastern part of the area, although dolomite units only host a small part of the ore. The felsic volcanic rocks in the ore body zone are strongly altered and secondary minerals such as magnetite, actinolite, chlorite or a quartz-pyrite-sericite assemblage preserve relics of the volcanic textures. The ore bodies of the Jalal Abad iron deposit are controlled by NE–SW trending faults, whereas N–S and E–W trending faults have a less important role. The form of ore bodies is also controlled by the contact zone and the fracture in volcano-sedimentary units and most of these are massive, layered, lenticular and irregular in shape.

The grade of ore varies from 30 to 50 wt. % Fe. Ore minerals are mainly magnetite, followed by apatite, pyrite, hematite, chalcopyrite and a small amount of pyrrhotite, bornite, gold and cobaltite. Gangue minerals are actinolite, calcite, dolomite, and a small amount of chlorite, epidote, and talc. The ores commonly have euhedral and subhedral granular, xenomorphic granular, reaction rim, and lattice-like textures. They also have disseminated, massive, striped-banded, mottled, crystal cave, and brecciated structures. Wall rock alteration is widespread in the mining area, and shows a close relationship with the ore bodies. Three stages of iron oxide Cu–Au mineralization are observed according to mineral assemblages and metasomatism producing an iron oxide stage (magnetite + actinolite + apatite + pyrite + quartz + chlorite) close to the gabbro-diorite, followed by the copper stage (pyrite + chalcopyrite + arsenopyrite + cobaltite + quartz + calcite) and the supergene stage (hematite + covelite + talc + Azurite + malachite + goethite) within the volcano-sedimentary host rock. The iron oxide stage is associated with three main alteration zones, from deep to shallow, of sodic-calcic (actinolite + albite ± chlorite), potassic (K-feldspar + biotite) and sericitic and silicic, and calcium (dolomite + calcite + epidote) alteration, which are controlled by NW trending faults. The sodic-calcic alteration is characterized by massive, vein-type, spotty and disseminated actinolite, which is for the most part common at deep levels, formed during iron oxide stage mineralization in association with magnetite, pyrite, apatite and minor amounts of zircon (Fig. 3g). Potassium

silicate alteration is characterized by biotite and K-feldspar in felsic volcanic rocks (Fig. 3h), which is developed at moderate to shallow levels. The sericitization and silicification alteration is represented by sericite, quartz, muscovite and hematite. Plagioclase and K- feldspar in felsic volcanic rocks are replaced by clay minerals and sericite. This alteration is common in shallow levels and is mostly associated with malachite mineralization, whereas silicification is in the form of veins and vugs of quartz in magnetite ore and host rocks. The Ca-alteration zone is represented by minerals such as dolomite, calcite and epidote replacing or overprinting earlier minerals. Dolomites formed as coarsely crystalline dolomite and saddle dolomite adjacent to the iron ore bodies. Saddle dolomite is normally associated with magnetite and occurs as veins and open space fillings.

Petrography

Petrographically, Jalal Abad volcanic rocks are classified into rhyodacite, rhyolite, tuff and ignimbrite, whereas most intrusions are granodiorite. Rhyolite displays rounded phenocrysts of quartz in a uniformly aphanitic and vuggy groundmass in hand samples (Fig. 3i). It has porphyritic textures and contains phenocrysts of biotite (5–7%), sanidine (~5–10%), and quartz (47%) set in a cryptocrystalline-felsite groundmass. The sanidine phenocrysts are characterized by idiomorphic to sub-idiomorphic shape with sieve and polysynthetic twinning textures which have been altered to sericite. The accessory minerals are biotite, titanite and iron oxides such as magnetite, ilmenite and hematite, whereas calcite, sericite, chlorite and hematite are secondary minerals.

Rhyodacite has a faulted contact with sedimentary (dolomite) rocks of the Rizu Formation (Fig. 3b) and shows aphyric to porphyritic textures in samples located close together in the field, with plagioclase (~50%), quartz (27%) and alkali feldspar (9-13%) phenocrysts set in a microcrystalline to cryptocrystalline groundmass of quartz, intergrowths of sodic plagioclase and K-feldspar. Quartz with resorbed texture is the main phenocryst and plagioclase is altered to epidote and calcite, whereas K-feldspar is altered to sericite. Apatite, biotite and iron oxides are accessory minerals, while calcite, sericite, hematite and chlorite are secondary minerals.

The ignimbrite occurs between rhyolitic rocks. It is white to red in color and contains abundant grey, aligned, and lenticular fiammes (Fig. 3c and j). The ignimbrites typically are composed of angular crystals of quartz, plagioclase, K-feldspar and crystal fragments set in a laminated tuffaceous matrix. Quartz crystals are generally corroded and have a thin overgrowth of quartz and sericite. The matrix consists of quartz, feldspar and iron oxides. Fiammes are easily

identified at the hand specimen and microscopic scale. Flattened pumice clasts or fiamme, ranging from 0.1–4 mm in diameter, are generally filled by sericite and quartz. The flattening orientation of the pumice is indicative of the diagenetic compaction orientation of the ignimbrites.

Welded tuffs consist predominantly of quartz, minor feldspar crystals and crystal fragments, set in a fine quartzofeldspathic matrix (Fig. 3k). The groundmass of the welded tuffs is extensively devitrified and recrystallized, which has transformed a vitroclastic texture to a fine crystalline matrix of anhedral quartz and K-feldspar.

Granodioritic rocks have porphyritic to granular textures and contain euhedral to subhedral phenocrysts of quartz (25%), K-feldspar (30%), plagioclase (35%), amphibole and biotite (3–8%) (Fig. 3l). Subhedral to anhedral K-feldspar (0.5–2 mm) grains are usually anhedral, occurs interstitially between plagioclase grains and are partly replaced by clay minerals. Magnetite, ilmenite, zircon and apatite are accessory minerals, while mafic minerals are replaced by secondary minerals such as chlorite and calcite.

4. Results

We studied >100 samples petrographically, 19 for whole-rock chemical analysis, two for LA-ICPMS U-Pb zircon ages, two for Lu-Hf analysis and eight for Sr-Nd isotopes. We selected fresh samples for whole-rock geochemistry. Analytical details are presented in supplementary files.

4.1. Whole-rock geochemistry

Fifteen samples of volcanic rocks (rhyolite and rhyodacite) and volcano-sedimentary rocks (tuff and ignimbrite) underwent whole-rock elemental analysis. While many magmatic rocks from the Jalal Abad have experienced surface alteration, relatively fresh samples were selected for major, trace and rare earth element (REE) analyses. The results of major oxides and trace elements in the different volcanic rocks are presented in Supplementary Table 1.

The effects of alteration are revealed by moderate loss-on ignition (LOI) measurements for all igneous rocks of Jalal Abad (1.0–3.8 wt. %). Major elements are re-calculated on volatile-free basis to avoid any misinterpretation arising from the alkali and large ion lithophile elements (LILE), which are more mobile during alteration processes and we use immobile trace elements

for classification. Most rhyolites and rhyodacites have lower SiO_2 contents (64.1–72.5 wt. %) and Zr/Ti ratios (0.01–0.18) than the ignimbrite (73.5–76.4 wt. % and 0.21–0.22, respectively), but similar to those values for tuff (71.2–71.5 wt. % and 0.11–0.13, respectively). Measured MgO contents are 0.47–0.93 wt. % in the rhyolite and rhyodacite, 0.20–0.45 wt. % in the ignimbrite, 0.43–1.40 wt. % in the tuffs. Relatively variable Al_2O_3 concentrations occur in the rhyolite and rhyodacite (11.7–20.5 wt. %) but is constant in the ignimbrite (11.2–11.3 wt. %) and in the tuffs (12.4–14.7 wt. %). Low Fe_2O_3 content occurs in the rhyolite (1.0–5.2 wt. %), ignimbrite (0.7–2.2 wt. %) and tuff (2.9–4.5 wt. %). Granodiorite samples are characterized by 68.6–71.2 wt. % SiO_2, 0.55–1.75 wt. % MgO, and Zr/Ti ratios of 0.04–0.28. They also have relatively constant Al_2O_3 (12.9–14.5 wt. %) and low Fe_2O_3 (3.1–4.2 wt. %) contents.

Based on an Nb/Y vs. Zr/TiO_2 diagram (Pearce 1996), all samples fall in the rhyolite and rhyodacite-dacite fields (Fig. 5a). They also demonstrate calc-alkaline and high K-calc-alkaline and shoshonite affinity, and all plot in the calc-alkaline rhyolite-dacite field on a plot of Co vs. Th (Hastie et al., 2007) (Fig. 5b). According to the Co vs. Th diagram (Fig. 5b) (Hastie et al. 2007), all granodiorite and volcanic rocks classify as medium- to high-K calc-alkaline series.

The REE patterns (Fig. 6a and c) normalized to chondritic values (McDonough & Sun, 1995) exhibit LREE/HREE enrichment and a negative Eu anomaly (Eu/Eu* = ~0.4–0.7). Calculated $(La/Yb)_N$ ratios vary from 6.6 to 7.9 in the rhyolite/rhyodacite, 6.6 to 29.1 in the ignimbrite/tuff and 6.5 to 14.1 in the granodiorite. The trace-element signatures of the studied granodiorite, volcanic and volcano-sedimentary rocks are presented as N-MORB-normalized (McDonough & Sun, 1995) spider plots (Fig. 6b and d). Most of the samples show enrichment in LILEs and depletion in HFSEs with negative anomalies in Nb, Sr, Ti. The geochemical features of granodiorites and rhyolite/rhyodacite, including high K calc-alkaline features, depletion in Nb, Ti and LILEs, and high LREE/HREE ratios, show affinity to continental arc magmatic rocks (Ducea et al., 2010; Moghadam et al., 2014)).

4.2. U–Pb zircon ages

Zircons from two representative igneous samples from host volcanic rocks of the Rizu series ZRD-12 (rhyolite) and intrusive rocks of ZRD-16 (granodiorite) were analyzed using LA-ICP-MS, with all data listed in Supplementary Table 2 and shown in Figure 7.

Rhyolite (sample ZRD-12)

Rhyolite sample ZRD-12 produced concordant ages from 25 separated zircon grains. Most are colorless, euhedral to subhedral and prismatic in shape, and characterized by regular concentric zoning in CL imagery. They range in length from 50 to 400 μm, with length to width ratios between 1:1 and 4:1. These zircons contain U (194–1811 ppm) and Th (71–663 ppm) contents and Th/U ratios of 0.3 to 1.0. All these characteristics are consistent with the zircons being of magmatic origin (Hoskin & Schaltegger, 2003). Twenty-five analyzed grains form a cluster with weighted mean ages of 552.3 ± 3.2 Ma (MSWD = 2.1) (Fig. 7a). One zircon core produced a $^{206}Pb/^{238}U$ age of 2101 ± 53 Ma, which is interpreted as the age of the crustal protolith that melted to form the lava.

Granodiorite (sample ZRD-16)

Twenty zircon grains from granodiorite sample ZRD-16 were analyzed for U–Pb ages (Supplementary Table 2). Most separated zircon grains are colorless, euhedral to subhedral prismatic, and characterized by regular concentric zoning in CL images. They range in length from 100 to 200 μm, and have length to width ratios between 1:1 and 2:1. Their U and Th contents are 153–654 ppm and 86–692 ppm, respectively. Most Th/U ratios range from 0.4 to 1.0, which are characteristic of magmatic zircons (Belousova et al., 2002). Zircons from sample ZRD-16 yielded a concordia age of 536.9 ± 2.7 Ma (MSWD = 2.5) (Fig. 7b), which is interpreted as the crystallization age of this granodiorite. One zircon core shows a $^{206}Pb/^{238}U$ age of 2180 ± 24 Ma, which is inferred to be the age of the crustal protolith.

4.3. Zircon Hf–O isotopes

The measured $^{176}Lu/^{177}Hf$ and $^{176}Hf/^{177}Hf$ ratios and $\delta^{18}O$ values of zircons in magmatic rocks of Jalal Abad are summarized in Supplementary Table 3. The $^{176}Hf/^{177}Hf$ ratios are 0.282423–0.282684 and 0.282340–0.2825869 for the granodiorites and rhyolite, respectively. The εHf(t) values for zircons from volcanic rocks have variable εHf(t) values of −3.9 to +3.9 (Fig. 8a). Zircons from granodiorite have variable εHf(t) values of –1.2 to +6.3. Crustal model ages of zircons (T_{DM}^{C}) from both volcanic and plutonic rocks of Jalal Abad vary between 0.9 and 1.7 Ga, except one point with a T_{DM}^{C} age of 3.4 Ga. (using $^{176}Lu/^{177}Hf$ = 0.015; Griffin et al., 2004). The $\delta^{18}O$ value of zircons from the volcanic rocks varies between 5 and 8.8 ‰, whereas granodiorites show $\delta^{18}O$ values of 3.3 to 8.7 ‰ (Fig. 8b). These values are slightly higher than the $\delta^{18}O$ typical of zircons from mantle-derived melts (~5.3 ‰; Eiler et al., 2000).

4.4 Whole rock Sr–Nd isotopes

Eight bulk-rock samples (two granodiorites, two rhyolites, two tuffs, and two ignimbrites) from the Jalal Abad were examined for Sr–Nd isotopes to determine their modes of origin (Supplementary Table 4). Initial $^{87}Sr/^{86}Sr$ and $^{143}Nd/^{144}Nd$ ratios for these rocks were re-calculated based on 552 Ma and 537 Ma crystallization ages for rhyolite and granodiorite, respectively. The Jalal Abad rhyolites display initial Nd isotope ratios of 0.5116024–0.5116031 while ignimbrite and tuff have 0.5115023–0.5116042 values. εNd (552) of all samples show narrow variations between −4.6 to −5.6 and −6.2 to −8.2 for rhyolite and tuff/ignimbrite, respectively. They plot within the continental crust field (Fig. 8c) on a εNd (t) vs. $^{87}Sr/^{86}Sr$ diagram and give depleted mantle model ages (T_{DM}) of 1.6–1.8 Ga (Supplementary Table 4). The Jalal Abad granodiorite show initial Nd isotope ratios of 0.5115500–0.5115678, and εNd (537) of all samples show narrow variations between −7.4 and −7.7. They also plot within the continental crust field (Figure 9) of εNd (t) vs. $^{87}Sr/^{86}Sr$ diagram and give T_{DM} of 1.8 Ga (Supplementary Table 4).

5. Discussion

The new data presented in this study offers new understandings into several features of Cadomian magmatism within Iran: 1 – the magma sources and petrogenetic processes involved during generation and evolution of the Jalal Abad magmatic rocks; 2 – crustal architecture in the Iranian Cadomian arcs; 3 – the geodynamic significance of the Cadomian magmatic arc; and 4 – implications for the metallogeny of the Jalal Abad.

5.1. Magma source and petrogenesis

The Jalal Abad magmatic rocks are comprised mainly of pyroclastic rocks intercalated with lava (~552 Ma) and intruded by younger granitoid intrusion (~537 Ma). Intermediate and silicic lavas tuffs and ignimbrites comprise >90 vol. % of the Jalal Abad magmatic rocks. Basalts and mafic intrusive rocks with Silurian ages (Vesali et al., 2020) are also present. Jalal Abad intermediate to felsic rocks have high-K calc-alkaline to shoshonitic signatures and show geochemical characteristics of I-type granitoids.

The magmatic rocks of Jalal Abad are characterized by negative Nb, Ta, Ti anomalies, and are strongly enriched in incompatible elements, including Rb, Th, U, K and LREE in a primitive mantle-normalized multi-element diagram (Sun and McDonough, 1989) (Fig. 5), which are typical features of subduction-related magmas (Khedr and Arai, 2016). Incompatible trace

elements, such as Ta, Th and Nb, show similar behaviors during melting and fractional crystallization, but are decoupled by the subduction process. Ytterbium is often used as a normalizing factor to minimize the effects of fractional crystallization and crystal accumulation (e.g. Pearce and Peate, 1995; Pearce et al., 2005). Thus, Th/Yb and Ta/Yb ratios were used for evaluation of the mantle metasomatism by slab-derived components. Since the addition of subducted components (e.g. sediments) generally increases Th but not Ta or Yb, an increase in Th/Yb ratio with nearly constant Ta/Yb ratio reflects addition of slab-derived components (Pearce et al., 2005). The source enrichment signatures in the Rizu igneous rocks can be deciphered on a plot of Th/Yb vs. Ta/Yb (Pearce et al., 1990) (Fig. 9a), with high Th/Yb ratios indicating a lithospheric mantle source enriched by subduction components (Dilek et al., 2010). This is supported by a Pb/Ce vs. La/Yb plot (Fig. 9b) (Embey-Isztin et al., 1993) that suggests that the mantle source of Rizu volcanics was modified by subduction-related components, such as melts and/or fluids released from the subducting slab (e.g. Hawkesworth et al., 1991, 1997; Elliott et al., 1997; Dhuime et al., 2009; Hernandez-Uribe et al., 2020).

All major geochemical signatures of the Jalal Abad igneous rocks, including Nb depletion, LILEs (e.g., Cs, Rb, Th, U, Sr, K) and LREEs (e.g., La, Ce) enrichment (Pearce and Peate, 1995; Thirlwall et al., 1994), and high Ba/La (8.4–26.1) and low Nb/La (0.08–0.30) ratios compared to N–MORB (Sun and McDonough, 1989) indicate generation at a convergent plate margin. In particular, the felsic volcanic rocks of the Jalal Abad have high Zr (114–250 ppm), Hf (3.8–7.1 ppm) and Y (12–25 ppm) contents, which are typical of continental arc magmas. Even though these geochemical features indicate a crustal influence, the relative depletion of Nb and other HFSEs relative to the LILEs, and enrichment of LILEs may be related to downgoing slabs or inherited from anatexis of an existing arc above a subducting plate (Khedr and Arai, 2016). However, given the lack of S-type granite in the region, it is likely that crustal anatexis did not occur (Zhang et al., 2020). Isotopically, the Jalal Abad granodiorite and felsic volcanic rocks appear cogenetic. Thus, except for variation in the Sr isotope compositions of the granodiorite, variations in whole-rock Nd and zircon Hf values can be ascribed to the different degrees to which the juvenile melt interacted with continental crust.

High-K, I-type felsic rocks are likely derived from (1) melting of hydrous intermediate to mafic high-K meta-igneous rocks (e.g., (Roberts and Clemens, 1993); (Sisson et al., 2005); (2) mixing of mantle–derived magmas with crustal melts (e.g., (Hildreth et al., 1991); (Huang et al., 2013), or (3) fractional crystallization (FC) of mantle-derived magmas (Grove et al., 2005). The Jalal Abad rocks show high SiO_2 contents (64.1–76.4 wt. %), low MgO contents (0.2–1.9 wt. %)

and radiogenic Sr–Nd–Pb isotopes, signifying they did not equilibrate with the upper mantle. However, the occurrence of the alkaline mafic counterparts (gabbro) in Zarand near the study area (Sepidbar et al., 2020), confirm derivation of the Jalal Abad magmas from mantle melts via FC and/or mixing of mantle-derived magmas with crustal-derived materials. The Nd isotopic compositions of the Jalal Abad magmatic rocks are also somewhat similar and suggest cogenetic relationships.

Based on the Sr–Nd isotope characteristics and the enriched LILE and K signature of the Jalal Abad magmatic rocks, the source is thought to be an enriched subcontinental lithospheric mantle (SCLM) that resembles EM II (Hofmann, 1997). However, the lack of basaltic shoshonitic rocks – the melting products of SCLM – cannot be easily addressed with this hypothesis. Therefore, the Sr–Nd isotopic data and trace element features of the Jalal Abad units require interaction of the mantle-derived magmas with thick continental crust during ascent, storage and evolution. The wide range of Hf isotopic composition of the Jalal Abad zircon ($\varepsilon Hf = -3.9$ to $+8.1$) also precludes a simple evolution of the Jalal Abad magmas by fractional crystallization, but other mechanisms such as wall-rock assimilation can potentially explain the observed Hf isotope variation. Therefore, the heterogeneous distribution of the zircon Hf–isotope data, as well the isotopically heavy O isotopes of zircon (Fig. 8b) and the whole-rock Nd isotopic compositions of the Jalal Abad rocks indicate that mantle-derived magma and pre-existing crustal material were involved in their genesis. Given the lack of Cadomian ophiolites throughout Iran, the isotope signatures of mantle melt components in the region cannot be directly examined; however, whole-rock Nd and zircon Hf–isotope model ages suggest that c. 0.8–2.3 Ga old continental crust interacted with juvenile magmas, with the Jalal Abad magmatic rocks being mixing products of this interaction. Crustal outcrops with these ages (~0.8–2.3 Ga) are absent in Iran, but as the Late Neoproterozoic volcano–sedimentary rocks host the Jalal Abad deposits, we assume the Paleoproterozoic-Mesoproterozoic lower crust as the continental components. The presence of inherited cores in the zircons used for U–Pb dating confirm the role of a Paleoproterozoic–Mesoproterozoic lower crust.

As such, both whole-rock trace-element/isotope and zircon Hf–O isotopic modeling are consistent with an AFC process involving interaction between a thick continental crust and a mantle-like melt. The Posht-e-Badam block, which hosts the Jalal Abad magmatic rocks and associated mineralization, contains abundant outcrops of Cadomian basement, with

Paleoproterozoic-Mesoproterozoic lower crust components, indicating that this block may have experienced sustained AFC processes.

5.2. Crustal architecture in the Iranian Cadomian arcs

The Hf "crustal" model ages, or T_{DM}^{C}, of zircons from Cadomian magmatic rocks through Iran can be used to evaluate the age at which their host magmas were extracted from the presumed depleted-mantle source (cf. Griffin et al., 2002). The studied Cadomian magmatic rocks have various origins from different magmatic domains. Therefore, comparison of Hf isotopic results for these magmatic zircons is used to evaluate their origin. Published data along with new results signify that there is no important variation in the sources of various rocks from these magmatic zircons. As a result, all measured Hf isotopic compositions of magmatic zircons in western-northwestern (Golpayegan, Khoy-Salmas, Zanjan-Takab), northeastern (Torud, Taknar), and central Iran (Saghand) are considered together with Cadomian magmatic zircon from the southeast (Jalal Abad) for the subsequent discussion. The calculated T_{DM}^{C} ages of all zircons from different domains of Iran are shown as histograms (Fig. 10). The combined T_{DM}^{C} age histogram of magmatic zircons from northeastern domain mainly ranges from 1.0 to 1.8 Ga with a major peak at ~1.6 Ga, whereas those from western and northwestern Iran dominantly ranges from 0.8 to 3.4 with a major peak at ~1.4 Ga (Stockli et al., 2004; Gilg et al., 2006; Hassanzadeh et al., 2008). The T_{DM}^{C} age histogram of magmatic zircons from the southeastern domain – including Jalal Abad – mostly varies from 0.8 to 2.3 Ga with a major peak at ~1.1 Ga, whereas T_{DM}^{C} age histogram of Nd–Sr isotopic results from central Iran dominantly ranges from 0.9 to 3.4 with a major peak at ~1.4 Ga (Hassanzadeh et al., 2008).

Cadomian magmas in northwest Iran mainly comprise granitic to tonalitic gneiss, granitoid, migmatite, granulite, rhyolites, metagranites, orthogneisses and felsic dikes, and are characterized by mostly variable zircon εHf(t) values of −30.5 to +10 (Mohammadi et al., 2017). However, in northeast Iran (560–530 Ma) (Moghadam et al., 2015) and central Iran (550–530 Ma) (Mohammadi et al., 2016), the same Cadomian magmatic rocks show a wide range in zircon εHf(t) values (−43 to +18; Moghadam et al., 2017a), which are more variable than those from northwestern Iran. In addition, both northeast and northwest Iran contain components of the Cadomian magmatic flare-up at ~570–530 Ma, whereas intrusions in central Iran were mostly emplaced at ~550 to 530 Ma, with an increased contribution from mantle-derived melts trending from northeast and northwest Iran to central Iran. Such a pattern for central Iranian Cadomian rocks is interpreted to record slab breakoff of the Proto-Tethys Ocean

lithosphere and associated extensional basins beneath central Iran (Sepidbar et al., 2020). However, isotopic data suggests that Cadomian magmas interacted less with continental crust than later magmas in the Mesoproterozoic-Early Neoproterozoic (Fig. 10). A $^{176}Hf/^{177}Hf$ vs U–Pb age plot (Fig. 8a) suggests that AFC processes were more important during magmatism in the Mesoproterozoic–Early Neoproterozoic (3000–1000 Ma), whereas juvenile magmas became increasingly important in the Cadomian (600–500 Ma) (Fig. 11). The Mesoarchean–Early Neoproterozoic magmatic rocks (3000–1000 Ma) are extensively exposed in Iran, where the Cadomian rocks also crop out as parts of the extensive Proto-Tethys subduction-related magmatic activity (Moghadam et al., 2017).

5.3. Geodynamic significance of Cadomian magmatic arc

It is commonly suggested the Cadomian arc was established after final amalgamation of the Gondwana supercontinent (Foden et al., 2006; Cawood et al., 2007; Ramezani and Tucker, 2003; Hassanzadeh et al., 2008). This period of arc magmatism was also an important basement-forming episode for Turkey (Gürsu and Göncüoglu, 2005, 2006) and the Iranian terranes (Hassanzadeh et al., 2008; Jamshidi Badr et al., 2013). The Cadomian magmatic flare-up in Iran represents magmatic pulses (Moghadam et al., 2017c; Sepidbar et al., 2020) that formed during a ~100 Myr period, producing an Andean-type belt of intrusive and extrusive rocks now present in the northwest, northeast, central and southeast regions of the country. Our study confirms that intrusive and extrusive rocks of Jalal Abad emplaced at ca. 552 to 537 Ma and are related to the Cadomian magmatic flare-up. Roll back of the subducted oceanic lithosphere beneath central Iran (*e.g.*, Moghadam et al.,2018; Sepidbar et al., 2020) is suggested to have caused these Cadomian magmatic activities throughout Iran, leading to compressional orogenic movements and subsequent high magma fluxes at 600–500 Ma (Moghadam et al., 2017c). Slab rollback may have been especially important because this is routinely associated with extension, crustal thinning and juvenile crustal addition (Miskovic and Schaltegger, 2009). Slab roll-back is the most important cause of upper plate extension and has produced elevated rates of magma generation in nearly all arcs worldwide (Ducea et al., 2017).

A large part of the basement of Central Iran, including Bafq and Jalal Abad regions, contains variably deformed and metamorphosed supracrustal rocks of the Neoproterozoic Morad series, Early Cambrian Rizu series, and volcano-plutonic rocks of Cadomian magmatic arc that lie on Cadomian crystalline basement (Moghadam et al., 2016a, b; 2017). In central Iran, Cadomian rocks occur along an arcuate and fault-bounded Kashmar-Kerman volcano-plutonic zone

within the Poshte-Badam block (Ramazani, 1997; Ramazani and Tucker., 2003). Extensive U–Pb zircon dating of igneous rocks throughout the Kashmar-Kerman zone and dating results in this study demonstrates three major periods in the geodynamic evolution of Cadomian arc magmatism in central Iran (Ramazani.,1997; Ramazani and Tucker., 2003). The early stage is characterized by development of a Cordilleran-type continental magmatic arc and emplacement of several granitic intrusions between 610 and 540 Ma (Ramazani and Tucker., 2003). This period of Cadomian arc magmatism was introduced by Ramazani and Tucker (2003) as a plutonic arc stage that was associated with emplacement of the main body of Cadomian granite plutons, which were subsequently deformed, such as Boneh-Shurow granit-orthogneiss (542 ± 9 Ma), Bornanvard intrusion, the Zaman Abad granite-gneiss, and the Poshteh Sorkh granite-gneiss. Cadomian plutonic rocks are metaluminous and have a high-K calc-alkaline affinity, and so show most similarity to I-type granites (Ramazani and Tucker, 2003).

Arc plutonism in the KKTZ was followed soon afterwards by the predominantly felsic to intermediate volcanism of the Cambrian Rizu Formation, which was emplaced over a short period of 533 to 525 Ma (Ramazani and Tucker, 2003). This event in the KKTZ is characterized by felsic arc volcanism and extensive volcanoclastic and pyroclastic eruptions, and sedimentation of thick sequences of volcano-sedimentary rocks in the ensialic to ensimatic back-arc basins (Ramazani.,1997; Ramazani and Tucker., 2003; Verdel,2007; Vesali and Esmailiy, 2016). The igneous crystallization age of the Rizu series in the Jalal Abad region (ca. 552–537 Ma) can be correlated with the first and second major period of Cadomian arc magmatism in the KKTZ. Slab retreat and extension following slab roll-back are thought to have been responsible for back-arc basin formation in Europe (i.e. the Rheic Ocean; Nance et al., 2010) and a series of the extensional ensialic back-arc basins in Iran and Turkey (Moghadam et al.,2016a, b; 2017). The development of the Cadomian arc was accompanied by formation of an ensialic back-arc basin, where the deposition of the Cambrian volcano-sedimentary rocks (Rizu, Desu, Ravar, Derin and Hormuz series) occurred (e.g. Linnemann et al., 2008).

Previous studies have shown that subduction-related arcs and back-arc basins were common throughout the KKTZ at ca. 550–525 Myr, as part of a much wider domain extending from Central Iran (KKTZ) and Bafq to the Takab in NW of Iran (Ghorbani, 2003). Our results are consistent with an interpretation that the Jalal Abad volcanic and plutonic rocks as well as associated thick sequences of sedimentary rocks formed in an extensional basin behind the

Cadomian magmatic arc. This basin seems to have developed during the Ediacaran at ca. 570-560 Ma with the deposition of Ediacaran Morad to Lower Cambrian Rizu-Dezo sedimentary rocks and seems to have become magmatically active at ca. 550–535 Ma, as shown by the formation of both high K calc-alkaline-shoshonitic magmatic rocks. The opening and spreading of back-arc basins likely occurred parallel to the convergence (Proto-Tethyan) margin (Nabatian et al., 2013). Thus, we suggest that southward subduction of the Proto-Tethys oceanic lithosphere produced an Andean type magmatic arc along the northern Iranian Plate, where equivalent volcanic and plutonic rocks formed at the active continental margin of the Arabian Plate. Rollback of the subducting Proto-Tethys oceanic lithosphere resulted in extension and opening of an intra-arc basin along the northern margin of the Iranian Plate (Moghadam et al., 2018; Sepidbar et al., 2020). The intrusion of the mafic dykes of the Jalal Abdad between 560 and 545 Ma as well as andesitic extrusions emplaced at around 550 Ma may be related to this extension. Extension and crustal thinning permit decompression melting of the SCLM or sub-arc mantle beneath the back arc. The new isotopic data from this study emphasize that the Jalal Abad calc-alkaline igneous rocks are connected to the pooling of mafic magmas in the continental crust of the Poshte Badam block, producing thermal anomalies and reworking of the Poshte Badam crust (Fig. 14)

4.4. Implications for the metallogeny of the Jalal Abad

Several iron-oxide deposits occur in the Saghand-Bafgh-Zarand district, hosted by Cadomian volcanic and sedimentary units, and these define an important iron metallogenic province in central Iran. As some critical data for the conditions of ore formation (e.g., isotopic data, fluid inclusion data) are unavailable, we can only place broad constraints on the metallogenesis by using basic geological and mineralogical characteristics. The orebodies of Jalal Abad are composed of high-grade massive ores, as well as low- to moderate-grade ores that include banded, brecciated, and disseminated ores. The massive magnetite orebodies, which make up the major mineralization at Jalal Abad, generally have sharp contacts with their host rocks. In addition, the vesicular-like texture, identified as a characteristic of magmatic ores in other iron deposits (Henríquez and Martin, 1978), is also locally developed in the Jalal Abad orebodies. The brecciated ore, with angular fragments of volcanic host rock cemented by magnetite, can plausibly be interpreted as resulting from an explosion of magma, caused by a sudden release of volatiles in response to decreasing pressure during ascent to near surface levels. The various forms of alteration associated with the Jalal Abad orebodies are characterized by a suite of metasomatism that range from an early Na–Ca–Fe alteration, overprinted by a high-

temperature K–Fe alteration, to a dolomitization, similar to those found in IOCG deposits (Hitzman et al., 1992; Williams et al., 2005). However, the occurrence of copper mineralization confirms the Jalal Abad orebodies as being categorized as an IOCG *sensu stricto* deposit (Chen, 2013; Williams et al., 2005).

Magnetite commonly occurs as anhedral–subhedral crystals or as fine-grained aggregates, and magnetite with replacement textures is rare. Notably, dendritic and platy forms of magnetite are present at Jalal Abad, similar to those observed at El Laco (Henríquez and Martin, 1978) and Kiruna, Sweden (Nyström, 1985; Nyström and Henríquez, 1989, 1994) where they were suggested to be the product of rapid crystallization during quenching, and diagnostic of a magmatic origin. This viewpoint was supported by the experiment of Philpotts (1967), in which dendritic magnetite developed as a result of rapid crystallization from a magnetite–fluorapatite system. For example, in Kiruna-type deposits, platy forms of magnetite are found mainly within the high-grade portions of the Jalal Abad orebodies, consistent with a magmatic origin for these ores. It is important to keep in mind that the interpretation of such features can be somewhat ambiguous and controversial. As noted by Rhodes et al. (1999), dendritic textures may be indicative of ultra-rapid cooling, but not necessarily of a melt (Sillitoe and Burrows, 2002). In general, the Jalal Abad magnetite ores share mineralogical features with the well-known magnetite deposits and magnetite–apatite deposits in the Chilean iron belt. A magmatic origin for the Jalal Abad deposit is therefore very plausible, based on the mineralogical evidence. The iron mineralization at Jalal Abad is spatially related to intermediate–mafic magmatic rocks, and in some cases a genetic link between them has been established (Mehrabia et al., 2019).

As noted above, melting of a mantle wedge, fertilized by fluids released from subducted oceanic crust and interaction of these mantle–derived magmas with thick continental crust during ascent, storage and evolution, is the most likely origin of the ore-related magmatism (Groves et al., 2010). The cause of the separation of Fe-rich melts (or fluids) from the arc magma is not known. It has been speculated that silicate liquid immiscibility, caused by crystal fractionation, magma mixing, an abrupt change in oxygen fugacity, and/or an introduction of phosphorus, may lead to the release of an oxidized melt from silicate magma (Hou et al., 2009). This model has been proposed for some of the magnetite–apatite deposits in the Chilean iron belt (Nyström and Henríquez, 1994; Travisany et al., 1995) and Kiruna (Frietsch, 1978). The occurrence of large amounts of the apatite as a gangue mineral is conspicuous in Kiruna-type deposits. Apatite in the Jalal Abad district occurs as an accessory phase in iron oxide stage

assemblages, and it has spatial association with the iron mineralization. This seems, therefore, the model involving immiscible magmatic liquids caused by the introduction of phosphorus cannot be completely excluded. However, Lledó (2005) has shown experimentally that even P_2O_5-poor andesitic magmas could readily generate immiscible Fe–P-oxide melts, owing to the strong melt polymerization characteristics of the final stages of crystallization (Chen et al., 2010b). This would be a viable mechanism to generate immiscible Fe-rich melts from parental magma, which were responsible for the iron mineralization at Jalal Abad. An alternative model involves unmixing of H_2O–CO_2–NaCl ± $CaCl_2$–KCl magmatic-hydrothermal fluids, caused by decreases in temperature and/or pressure (Pollard, 2001), to result in the precipitation of iron oxides and associated K–Na–Ca alteration in the Jalal Abad iron deposit.

As such, the results presented here indicate that the Jalal Abad deposit is a typical IOCG magnetite deposit, as described by Dill (2010), and that it formed in a subduction setting during the Cadomian. The mantle wedge overlying the subduction zone was fertilized by fluids from the subducted slab, and the consequential partial melting of the wedge probably resulted in the generation of hydrous, metalliferous, and fertile mafic magma (Groves et al., 2010; Li et al., 2013) This is consistent with evidence of Ti-rich ferropicritic magmatism during arc magmatism in Arabian Nubian Shield (see Khedr et al., 2020). The Jalal Abad iron deposit was formed from Fe-rich melts (or fluids) that were derived from the mafic magma and channeled along major faults and fractures within the volcano-sedimentary rocks of Rizu Formation. The source of the iron can ultimately be ascribed to the mafic magmas derived from the mantle wedge, which may contain ~7.5–10.5 wt. % FeO if generated at fore-arc mantle potential temperatures (Weller et al., 2019).

5. Conclusion

The Cadomian Jalal Abad magmatic rocks are part of a voluminous Cadomian magmatic arc in Iran, the southeastern Kashmar-Kerman tectonic zone. This zone is recognized as a Cadomian flare-up and associated mineralization dominated by calc-alkaline and shoshonitic rocks. The Jalal Abad magmatic rocks are characterized by high K_2O and enrichment in LREEs and LILEs, along with depletion in HFSEs, and resemble those erupting along active continental margins. These intrusive and extrusive rocks have similar geochemical and Sr–Nd isotope compositions, suggesting they are cogenetic and erupted during a ~15 Myr interval. The whole-rock Sr–Nd–Pb and zircon Hf–O isotope data show that the Jalal Abad magmatic

rocks probably formed from significant interaction of juvenile melts with old (~0.8–2.3 Ga) continental crust through AFC process.

Magnetite is the dominant primary iron-oxide mineral in the orebodies associated with Jalal Abad magmatic rocks, commonly occurring as anhedral–subhedral crystal or as fine-grained aggregate. Dendritic and platy magnetite is also present, mainly within high-grade massive ores, suggesting a magmatic origin for the Jalal Abad deposit. The alteration associated with the magnetite ores ranges from an Na–Ca alteration that may be overprinted by a high-temperature K alteration, to a late-stage alteration involving low-temperature hydration, similar to those found in IOCG deposits.

Acknowledgments

We gratefully acknowledge the support of the the Jalal-Abad mine during sampling and field work. We would like to thank Prof. Mohammad Zaki Khedr and an anonymous referee for their careful, incisive and constructive reviews for through review and constructive comment. Special thanks are also due to Profs. Nicolas Thebaud and Huayong Chen for their dedicated editorial work.

Figure captions

Fig. 1. Simplified geological map of Iran showing the distribution of Cadomian basement rocks, Paleozoic-Mesozoic volcano-sedimentary rocks, Cenozoic igneous rocks and Paleozoic-Mesozoic ophiolites as we as Saghand-Bafq-Zarand district.

Fig. 2. (a) Geological map of the in the Jalal Abad region with location of study area (modified after 1:100000 Davaran geological map); (b) Geological cross section of the Jalal-Abad iron ore deposit (modified after Technoexport, 1976).

Fig. 3. Field photographs of igneous rocks of the Rizu series in the Jalal Abad region. (a) White-colored interlayers of rhyolite to rhyodacitic tuffs and ignimbrite sheet occur between the rhyolitic (flow) layers; (b) field occurrence of rhyodacites and their relationship with overlying Desu limestones; (c) light-colored lense-shaped fiammes in the Jalal Abad ignimbrites; (d) field exposures of tuffs and their relationship with overlying Desu limestones, (e) emplacement of the granodiorite into volcanic rocks of the Rizu series; (f) drill core of iron oxide and related volcano-sedimentary host rocks; (g) Ca-Na metasomatism with actinolite (Act) in a magnetite ore body (drill core); (h) biotite (Bt) and orthoclase (Or) in potassic alteration in felsic volcanic rocks; (i) the engulfed margin of quartz crystals in the quartz porphyry rocks; (j) lense-shaped

fiammes in the Jalal Abad ignimbrites; (k) welded tuffs consist predominantly of quartz, minor feldspar crystals and crystal fragments, set in a fine quartzofeldspathic matrix; (l) granodioritic rocks have porphyritic to granular textures and contain quartz, K-feldspar, plagioclase, amphibole and biotite.

Fig. 4. Paragenetic sequence of iron oxide Cu–Au mineralization in the Jalal-Abad deposit.

Fig. 5. Zr/TiO2 *vs* Nb/Y (a) and Th *vs* Co (b) plots for the classification of magmatic rocks from Jalal Abad. Data for Cadomian calc-alkaline rocks come from (Badr *et al*. 2013; Balaghi *et al*. 2014; Moghadam *et al*. 2015, 2016, 2017c, 2020b).

Fig. 6. SiO_2 vs. selected major and trace element Harker diagrams for Sik Kuh and Bobak volcanic rocks.

Fig. 6. Chondrite-normalized rare earth element (a and c) and N-MORB-normalized trace element patterns (b and d) for the magmatic clasts from Jalal Abad. Chondrite and N-MORB normalized values are taken from (Sun and McDonough 1989).

Fig. 7. Concordia and weighted mean $^{206}Pb/^{238}U$ age plots for the investigated zircons from the Cadomian magmatic rocks from Jalal Abad.

Fig. 8. a) Initial Hf isotopic composition vs $^{206}Pb/^{238}U$ crystallization ages of the Jalal Abad magmatic rocks; b) Plot of $\delta^{18}O$ versus εHf(t) for Cadomian rocks of Jalal Abad and Iran (modified after Kemp et al. 2007), showing curves corresponding to magma evolution by crustal assimilation–crystallization (AFC). Hf_{PM}/Hf_C = ratio of Hf concentration in the parental magma (pm) to Hf concentration in crustal (c) rocks. Zircon Hf–O isotope data for Iran Cadomian rocks, Eocene Kurdistan juvenile gabbros and Nain ophiolite are from Moghadam et al. (submitted). The Kurdistan and Nain ophiolite zircons present mantle-derived juvenile melts and are for comparison to reveal crustal input in Cadomian rocks; c) Bulk rock Sr-Nd isotopic composition of the magmatic rocks from Jalal Abad.

Fig. 9. (a) Th/Yb vs. Ta/Yb diagram (Pearce, 1982) showing high Th/Yb ratio for the magmatic rocks which displays a lithospheric mantle source enriched by subduction components; (b) Plots of (a) Pb/Ce v. La/Yb for magmatic rocks of Jalal Abad.

Fig. 10. Histograms of T_{DM}^C ages of the Cadomian magmatic zircons in Iran. The data from Iran are from Moghadam et al. (2017) and references therein.

Fig. 11. $^{176}Hf/^{177}Hf$ (initial) vs zircon $^{206}Pb/^{238}U$. This shows that Cadomian magmas have less crustal influence with time and that Mesoproterozoic-Neoproterozoic igneous rocks show the greatest crustal influence.

Fig. 12. A schematic crustal column through the Cadomian arcs of in the Jalal Abad.

Supplementary Table Captions

Supplementary Table 1. Whole rock composition of the Chah-Gaz and Mishdovan alkaline and high-K calc-alkaline to shoshonitic rocks

Supplementary Table 2. Zircon U–Pb age results for the Jalal Abad Cadomian magmatic rocks.

Supplementary Table 3. Zircon Hf–O isotopic results for the Jalal Abad Cadomian magmatic rocks.

Supplementary Table 4. Whole rock Nd–Sr isotopic composition of the Jalal Abad magmatic rocks.

References

Abbo, A., Avigad, D., Gerdes, A., Gungor, T., 2015. Cadomian basement and Paleozoic to Triassic siliciclastics of the Taurides (Karacahisar dome, south-central Turkey): Paleogeographic constraints from U-Pb-Hf in zircons. Lithos 227, 122–139.

Balaghi, M.E., Mahmoud, S., Zhai, M.G., Habibollah, G., Mohammad, M., 2014. Zircon U-Pb ages, Hf isotopes and geochemistry of the schists, gneisses and granites in Delbar Metamorphic-Igneous Complex, SE of Shahrood (Iran): Implications for Neoproterozoic geodynamic evolutions of Central Iran. Journal of Asian Earth Sciences 92, 92–124.

Badr, M.J., Collins, A.S., Masoudi, F., Cox, G., Mohajjel, M., 2013. The U-Pb age, geochemistry and tectonic significance of granitoids in the Soursat Complex, Northwest Iran. Turkish Journal of Earth Sciences 22, 1–31.

Bookstrom, A.A., 1977. The magnetite deposits of El Romeral, Chile. Econ. Geol. 72, 1101–1130.

Chen, H.Y., Clark, A.H., Kyser, T.K., Ullrich, T.D., Baxter, R., Chen, Y.M., Moody, T.C., 2010a. Evolution of the giant Marcona-Mina Justa iron oxide-copper–gold district, southcentral Peru. Econ. Geol. 105, 155–185.

Chen, H.Y., Clark, A.H., Kyser, T.K., 2010b. The Marcona magnetite deposit, Ica, South-Central Peru: a product of hydrous, iron oxide-rich melts? Econ. Geol. 105, 1441–1456.

Daliran, F., 2002. Kiruna-type iron oxide-apatite ores and apatitites of Bafq district, Iran, with an emphasis on the REE geochemistry of their appetites. PGC Publishing, Linden Park, South Australia, pp. 303–320.

Ducea, M.N., Bergantz, G.W., Crowley, J.L., Otamendi, J., 2017. Ultrafast magmatic buildup and diversification to produce continental crust during subduction. Geology 45, 235–238.Eiler, J.M., Crawford, A., Elliott, T., Farley, K.A., Valley, J.W., Stolper, E.M., 2000. Oxygen isotope geochemistry of oceanic–arc lavas. Journal of Petrology 41, 229–256.

Embey-Isztin, A., Downes, H., James, D.E., Upton, B.G.J., Dobosi, G., Ingram, G.A., Harmon, R.S., Scharbert, H.G. (1993). The petrogenesis of Pliocene alkaline volcanic rocks from the Pannonian Basin; Eastern Central Europe*;* Journal of Petrology*,* 34 317–343.

Förster, H., Jafarzadeh, A., 1994. The Bafq mining district in Central Iran: a highly mineralized Infracambrian volcanic field. Econ. Geol. 89, 1697–1721.

Griffin, W.L., Wang, X., Jackson, S.E., Pearson, N.J., O'Reilly, S.Y., Xu, X., Zhou, X., 2002. Zircon chemistry and magma mixing, SE China: in-situ analysis of Hf isotopes, Tonglu and Pingtan igneous complexes. Lithos 61, 237–269.

Griffin, W.L., Belousova, E.A., Shee, S.R., Pearson, N.J., and O'Reilly, S.Y., 2004, Archean crustal evolution in the northern Yilgarn Craton: U–Pb and Hf-isotope evidence from detrital zircons: Precambrian Research, 131, 3–4, 231–282. doi:10.1016/j.precamres.2003.12.011

Grove, T.L., Baker, M.B., Price, R.C., Parman, S.W., Elkins-Tanton, L.T., Chatterjee, N., Muntener, O., 2005. Magnesian andesite and dacite lavas from Mt. Shasta, northern California: products of fractional crystallization of H_2O–rich mantle melts. Contributions to Mineralogy and Petrology 148, 542–565.

Gursu, S.,Moller, A., Goncuoglu,M.C., Koksal, S., Demircan, H., Koksal, F.T., Kozlu, H., Sunal, G., 2015. Neoproterozoic continental arc volcanism at the northern edge of the Arabian Plate, SE Turkey. Precambrian Research 258, 208–233.

Hernández-Uribe, D., Hernández-Montenegro, J.D., Cone, K.A. and Palin, R.M., 2020. Oceanic slab-top melting during subduction: Implications for trace-element recycling and adakite petrogenesis. *Geology*, *48*, 216-220.

Hassanzadeh, J., Stockli, D.F., Horton, B.K., Axen, G.J., Stockli, L.D., Grove, M., Schmitt, A.K., Walker, J.D., 2008. U-Pb zircon geochronology of late Neoproterozoic-Early Cambrian granitoids in Iran: Implications for paleogeography, magmatism, and exhumation history of Iranian basement. Tectonophysics 451, 71–96.

Hastie, A.R., Kerr, A.C., Pearce, J.A., and Mitchell, S.F., 2007, Classification of altered volcanic island arc rocks using immobile trace elements: Development of the Th-Co discrimination diagram: Journal of Petrology, v. 48, no. 12, p. 2341–2357. doi:10.1093/petrology/egm062.

Hawkesworth, C.J., Hergt, J.M., Ellam, R.M. & McDermott, P. (1991). Element fluxes associated with subduction related magmatism; *Phil. Trans. R.Soc, London* **335** 393–405.

Hawkesworth, C.J., Turner, S.P., McDermott, F., Peate, D.W. & Van Calsteren, P. (1997). U–Th isotopes in Arc magmas: implications for element transfer from the subducted crust. *Science 276*, 551–555.

Hildreth, W., Halliday, A.N., Christiansen, R.L., 1991. Isotopic and Chemical Evidence Concerning the Genesis and Contamination of Basaltic and Rhyolitic Magma beneath the Yellowstone Plateau Volcanic Field. Journal of Petrology 32, 63–138.

Hofmann, A.W., 1997. Mantle geochemistry: the message from oceanic volcanism. *Nature*, *385*, 219-229.

Horton, B.K., Hassanzadeh, J., Stockli, D.F., Axen, G.J., Gillis, R.J., Guest, B., Amini, A., Fakllari, M.D., Zamanzadeh, S.M., Grove, M., 2008. Detrital zircon provenance of Neoproterozoic to Cenozoic deposits in Iran: Implications for chronostratigraphy and collisional tectonics. Tectonophysics 451, 97–122.

Hoskin, P.O and Schaltegger, U., 2003. The composition of zircon and igneous and metamorphicpetrogenesis, in Hanchar JM and Hoskin, PWO eds, Zircon: Mineralogical Society of America. *Reviews in Mineralogy and geochemistry, 53* 27–62.

Huang, F., Lundstrom, C.C., 2007. ^{231}Pa excesses in arc volcanic rocks: Constraint onmelting rates at convergent margins. Geology 35.

Khedr, M.Z., Arai, S., 2016a. Petrology of a Neoproterozoic Alaskan-type complex from the Eastern Desert of Egypt: Implications for mantle heterogeneity. Lithos, 263, 15–32. doi: 10.1016/j.lithos.2016.07.016.

Khedr, M.Z, El-Awady, A., Arai, S., Hauzenberger, C., Tamura, A., Stern, R.J., Morishita, T., 2020. Petrogenesis of the ~740 Korab Kansi mafic-ultramafic intrusion, South Eastern Desert of Egypt: Evidence of Ti-rich ferropicritic magmatism. Gondwana Reserch, 82, 48–***72.***

Linnemann, U., Pereira, F., Jeffries, T.E., Drost, K., Gerdes, A., 2008. The Cadomian Orogeny and the opening of the Rheic Ocean: The diacrony of geotectonic processes constrained by LA-ICP-MS U-Pb zircon dating (Ossa-Morena and Saxo-Thuringian Zones, Iberian and Bohemian Massifs). Tectonophysics 461, 21–43.

Mehrabi, B., Karimi Shahraki, B., Banks, D., Boyce, A., Yardley, B .W.D., 2019. Hydrothermal iron oxide-Cu-Au (IOCG) mineralization at the Jalal-Abad deposit, northwestern Zarand, Iran. Ore Geology Reviews 106, 300–317.

Miskovic, A., Schaltegger, U., 2009. Crustal growth along a non-collisional cratonic margin: A Lu-Hf isotopic survey of the Eastern Cordilleran granitoids of Peru. Earth and Planetary Science Letters 279, 303–315.

Moghadam, H.S., Khademi, M., Hu, Z.C., Stern, R.J., Santos, J.F., Wu, Y.B., 2015. Cadomian (Ediacaran-Cambrian) arc magmatism in the ChahJam-Biarjmand metamorphic complex (Iran): Magmatism along the northern active margin of Gondwana. Gondwana Research 27, 439–452.

Moghadam, H.S., Li, X.H., Stern, R.J., Santos, J.F., Ghorbani, G., Pourmohsen, M., 2016. Age and nature of 560-520 Ma calc-alkaline granitoids of Biarjmand, northeast Iran: insights into Cadomian arc magmatism in northern Gondwana. International Geology Review 58, 1492–1509.

Moghadam, H.S., Griffin,W.L., Li, X.H., Santos, J.F., Karsli, O., Stern, R.J., Ghorbani, G., Gain, S., Murphy, R., O'Reilly, S.Y., 2017a. Crustal Evolution of NWIran: Cadomian Arcs, Archean Fragments and the Cenozoic Magmatic Flare-Up. Journal of Petrology 58, 2143–2190.

Moghadam, H.S., Li, X.-H., Griffin,W.L., Stern, R.J., Thomsen, T.B., Meinhold, G., Aharipour, R., O'Reilly, S.Y., 2017b. Early Paleozoic tectonic reconstruction of Iran: Tales from detrital zircon geochronology. Lithos 268, 87–101.

Moghadam, H.S., Li, X.H., Santos, J.F., Stern, R.J., Griffin, W.L., Ghorbani, G., Sarebani, N., 2017c. Neoproterozoic magmatic flare-up along the N. margin of Gondwana: The Taknar complex, NE Iran. Earth and Planetary Science Letters 474, 83–96.

Nance, R.D., Gutierrez-Alonso, G., Keppie, J.D., Linnemann, U., Murphy, J.B., Quesada, C., Strachan, R.A., Woodcock, N.H., 2010. Evolution of the Rheic Ocean. Gondwana Research 17, 194–222.

Nyström, J.O., Henríquez, F., 1989. Dendritic magnetite and miniature diapir-like concentrations of apatite: two magmatic features of the Kiirunavaara iron ore. Geol. Foren. Stock. For. 111, 53–64.

Pearce, J.A. 1996. A users guide to basalt discrimination diagrams.

Pearce, J.A., Peate, D.W., 1995. Tectonic implications of the composition of volcanic arc magmas. Annu. Rev. Earth Planet. Sci. 23, 251–285.

Ramezani, J., Tucker, R.D., 2003. The Saghand Region, Central Iran: U-Pb geochronology, petrogenesis and implications for Gondwana Tectonics. American Journal of Science 303, 622–665

Roberts, M.P., Clemens, J.D., 1993. Origin of High-Potassium, Calc-Alkaline, I-Type Granitoids. Geology 21, 825–828.

Rossetti, F., Nozaem, R., Lucci, F., Vignaroli, G., Gerdes, A., Nasrabadi, M., Theye, T., 2015. Tectonic setting and geochronology of the Cadomian (Ediacaran-Cambrian) magmatism in Central Iran, Kuh-e-Sarhangi region (NW Lut Block). Journal of Asian Earth Sciences 102, 24–44.

Sanchez-Garcia, T., Quesada, C., Bellido, F., Dunning, G.R., del Tanago, J.G., 2008. Two-step magma flooding of the upper crust during rifting: The Early Paleozoic of the Ossa Morena Zone (SW Iberia). Tectonophysics 461, 72–90.

Sepidbar, F., Shafaii Moghadam, H., Li, C., Stern, R.J., Jiantang, P., and Vesali, Y., 2020, Cadomian magmatic rocks from zarand (SE Iran) formed in a retro-arc basin: Lithos, p. 366–367

Sillitoe, R., 2003. Iron oxide-copper–gold deposits: an Andean view. Mineral. Deposita 38, 787–812.

Sisson, T.W., Salters, V., Larson, P., 2014. Petrogenesis of Mount Rainier andesite: Magma flux and geologic controls on the contrasting differentiation styles at stratovolcanoes of the southern Washington Cascades. Bulletin 126, 122–144.

Sun, S.-S., McDonough, W.S., 1989. Chemical and isotopic systematics of oceanic basalts: implications for mantle composition and processes. Geological society, London, special publications 42, 313–345.

Vesali, Y., Esmaeily, D., Sepidbar, F., Sheibi, M., Niromand, S., 2018. Petrology, geochemistry and tectonic setting of alkaline mafic rocks in the Jalal Abad area in the NW of Zarand (Kerman Province): Evidence for Paleo-Tethys rifting in the Central Iran. Journal of Petrology, 33, 1-20 (in Persian with English abstract).

Vesali, Y., Esmaeily, D., Moazzen, M., Chiaradia, M., Morishita, T., Soda, Y., & Sheibi, M. (2020). The Paleozoic Jalal Abad mafic complex (Central Iran): implication for the petrogenesis. Geochemistry. doi:10.1016/j.chemer.2020.125597

Weller, O.M., Copley, A., Miller, W.G.R., Palin, R.M. and Dyck, B., 2019. The relationship between mantle potential temperature and oceanic lithosphere buoyancy. Earth and Planetary Science Letters, 518, 86-99.

Zhang, Z., Ding, H., Palin, R.M., Dong, X., Tian, Z. & Chen, Y., 2020. The lower crust of the Gangdese magmatic arc, southern Tibet, implication for the growth of continental crust. Gondwana Research, 77, 136-146.

- The Jalal Abad magmatic rocks have identical zircon U–Pb ages of *ca* 552–537 Ma.
- Jalal Abad igneous rocks have high–K signature with identical whole rock and zircon isotopes.
- Assimilation of thick continental crust by mantle melts generated the Jalal Abad magmatic rocks.
- AFC processes were more important in the Mesoarchean–Early Neoproterozoic, whereas juvenile magmas became increasingly important in the Cadomian.